J Mater Sci (2022) 57:1936–1946

Electronic materials

Simple preparation of highly efficient $MA_xFA_{1-x}PbI_3$ perovskite films from an aqueous halide-free lead precursor by all dip-coating approach and application in high-performance perovskite solar cells

Zobia Irshad[1], Muhammad Adnan[1], and Jae Kwan Lee[1,2,*]

[1] Department of Chemistry, Graduate School, Chosun University, Gwangju 61452, Republic of Korea
[2] Department of Chemistry Education, Chosun University, Gwangju 61452, Republic of Korea

Received: 19 September 2021
Accepted: 3 January 2022
Published online: 12 January 2022

ABSTRACT

All sequential-dip-coating deposition of mixed organic cationic $MA_xFA_{1-x}PbI_3$ perovskite films from an aqueous non-halide lead precursor solution was effectively developed. Efficient crystal phase and surface morphologies of $MA_xFA_{1-x}PbI_3$ perovskite films were successfully realized by varying MAI/FAI molar ratios in precursor solution over as-prepared $Pb(NO_3)_2$ layer. The various grain sizes and boundaries as well as cubical lumps of $MA_xFA_{1-x}PbI_3$ perovskite crystal were also modulated after annealing at 120 °C of produced $MA_xFA_{1-x}PbI_3$ perovskite films formed with suitable concentrations of MAI and FAI solution. Interestingly, all-dip-coating-treated $MA_xFA_{1-x}PbI_3$ perovskite layers have no presence of δ-$FAPbI_3$ perovskites, even at low MAI insertion into the FAI solution. Efficient device performances and improved stability with a power conversion efficiency of $\sim$ 14.1% in perovskite solar cell devices with the all-dip-coating processed $MA_{0.5}FA_{0.5}PbI_3$ perovskite layers realized by incorporating $Pb(NO_3)_2$ layers into MAI/FAI (1/1 molar ratio) solution.

Introduction

Perovskite solar cells (PrSCs) based on organic–inorganic halide perovskites have been extensively studied in recent years because of their high PCEs, ease in fabrication and low preparation cost [1, 2]. The excellent performances of PrSCs devices take advantage of perovskite materials contained inorganic lead bridged cores with organic cationic species (alkylammonium) and anionic halide. Among, the direct band-gap material such as methylammonium

Handling Editor: Kyle Brinkman.

Zobia Irshad and Muhammad Adnan contributed equally for the first authorship.

Address correspondence to E-mail: chemedujk@chosun.ac.kr

https://doi.org/10.1007/s10853-022-06867-9

lead halide $MAPbX_3$ (X = I, Br or Cl) was employed at the preliminary phase of PrSCs by reacting with lead halide (PbX_2) and methylammonium halides (CH_3NH_3X, MAX). These perovskite materials are superior because of their broader light absorption range, lower exciton binding energy, adequate optical band-gap and higher charge transportation [3]. Although the $MAPbI_3$ perovskite material, having a direct bandgap of 1.57 eV, has been specifically employed as the light harvesters in PSCs, it was reported that $MAPbI_3$ perovskite films undergo degradation in light and heat mainly in the existence of solvents or humidity and possess inadequate short-circuit photocurrent density (J_{sc}) [4, 5, 6]. Moreover, when the temperature exceeds beyond 60 °C, the $MAPbI_3$ perovskite films faced phase transition behavior because of their lower crystallization energy. Recently, $FAPbI_3$ perovskite material incorporated formamidinium cation [$HC(NH_2)_2^+$, FA) has been considered as high-performing perovskite materials, because it possesses a higher photo- and thermal stability and lower bandgap (∼ 1.4 eV) to replace $MAPbI_3$ PrSCs [7, 8]. The $FAPbI_3$ perovskite layers are often prepared with the solution deposition process and required specific heating process to transform the deposited solution into a crystalline form. However, $FAPbI_3$ perovskite films show inherent instability and are found into two polymorphs states; a perovskite blackish phase (α-$FAPbI_3$) and a non-perovskite yellowish phase (δ-$FAPbI_3$). At ambient temperature, the black α-$FAPbI_3$ phase which is employed as a specific light-absorbing layer in PSCs devices [9] is so non-stable that it transforms into the perovskite-free yellow δ-$FAPbI_3$ phase readily [10]. By considering these, it seems that the $MAPbI_3$ and $FAPbI_3$ have specific drawbacks as absorption materials of PrSCs when used independently. Therefore, many research groups have explored extensively the usage of mixed organic-cation perovskite layers such as $MA_xFA_{1-x}PbI_3$ to overcome the disadvantages of PSCs devices with single cation perovskite films [11–13]. Mixed organic cation ($MA_xFA_{1-x}PbI_3$) perovskite layers have exhibited various advantages to further enhance the PCE and stability of PSCs films, because MA cation stabilizes the α-$FAPbI_3$ perovskite films and stops their conversion into δ-$FAPbI_3$ perovskites at room temperature [14]. Also, researchers have reported some extra-ordinary features of mixed organic-cationic perovskite films as an efficient light absorber: a high defect tolerance, a suitable tunable bandgap, a longer charge carrier diffusion lengths, higher absorption co-efficient and a bi-polar charge transport characteristics. These parameters are the key factors in improving the photovoltaic performance of PrSCs devices [1–4].

Up to date, PrSCs have attained great success via various strategies and the efficiency of PSCs devices boosted up to 25.2%, analogous to those of polycrystalline solar cells [3]. But still, it is challenging enough for industrial applications by advancing the advanced deposition technologies to minimize the threat of the size limitations caused by conventional spin-coating process as well as usage of detrimental organic solvents (DMSO and DMF), used to dissolve lead halide precursors. Very recently, we have reported an effective strategy to deposit methylammonium (MA) lead halide ($MAPbI_3$) perovskite materials by an advanced, simple, and unique all sequential-dip-coating (SDC) method from an aqueous halide-free lead precursor, $Pb(NO_3)_2$ for efficient PrSCs. The SDC approach proves better to efficiently dominate the size limitations caused by conventional spin-coating process and can produce larger-area device fabrication of efficient perovskite films prepared with an aqueous $Pb(NO_3)_2$, which was being used because of its affinity with non-toxic, low cost and environmental solvents, like water. Because of these, in the present study, we have also made an effort to employ the all sequential-dip-coating approach to prepare $MA_xFA_{1-x}PbI_3$ perovskites from an aqueous halide-free $Pb(NO_3)_2$ as a simple, low-cost and environmentally benign method. We have also modulated the phase and surface crystallinity of $MA_xFA_{1-x}PbI_3$ perovskites from all sequential-dip-coating approaches to fabricate an efficient PSCs device.

Herein, we effectively established an all-sequential-dip-coating approach of efficient $MA_xFA_{1-x}PbI_3$ perovskite films prepared by an aqueous non-halide lead precursor solution. During sequential dip-coating of $Pb(NO_3)_2$ layer deposited over a ZnO covered c-TiO_2 bilayer substrate, efficient phase and surface morphologies of $MA_xFA_{1-x}PbI_3$ perovskite films were successfully realized by varying MAI/FAI molar ratios in precursor solution over as-prepared $Pb(NO_3)_2$ layer. The various grain sizes and boundaries (along-with crystal growth) as well as cubical lumps of $MA_xFA_{1-x}PbI_3$ perovskite crystal were also demonstrated after annealing at 120 °C of as-

prepared $MA_xFA_{1-x}PbI_3$ perovskite layers obtained with appropriate concentrations of MAI and FAI solution. Interestingly, all-dip-coating processed $MA_xFA_{1-x}PbI_3$ perovskite films have no presence of δ-$FAPbI_3$ perovskites, even at low MAI insertion into the FAI solution, and have superior surface coverages. The fabricated PSCs devices ($MA_xFA_{1-x}PbI_3$) exhibited a superior performance with improved stabilities in planar heterojunction (PHJ) architecture with a notable PCE value of 14.1% all sequential-dip-coating deposition processed $MA_{0.5}FA_{0.5}PbI_3$ perovskite films prepared by incorporating as-deposited $Pb(NO_3)_2$ layer in MAI/FAI (1/1 molar ratio) solution.

Experimental section

Fabrication of $MA_xFA_{1-x}PbI_3$ perovskite films

The $MA_xFA_{1-x}PbI_3$ perovskite layer deposited via aqueous $Pb(NO_3)_2$ SDC goes along with SSIER repetition. In a standard process, FTO substrates having a ZnO and cp-TiO bilayer were primarily bathed into a 0.1 M solution of Pb $(NO_3)_2$ (Sigma-Aldrich, 99.9%) dissolved in ethanol/water (2:1, v/v) for 30 s. After that substrate was rinsed with deionized water and ethanol and then annealed at 120 °C for 10 min, and finally achieved semi-transparent layer on top of the substrate. The 0.63-M MAI and 0.58-M FAI solution was dissolved in isopropanol. The MAI/FAI mixed-halide perovskite layers were fabricated by using various concentrations of MAI/FAI of (0.7/0.3, 0.6/0.4, 0.5/0.5, 0.4/0.6, and 0.3/0.7), respectively, in isopropanol for 30 s then dried at 120 °C for 10 min under controlled humidity of less than 20%. This process developed single SSIER cycle. There were several SSIER repetitions to occur to complete the reaction between $Pb(NO_3)_2$ and MAI/FAI.

PrSC device fabrication

Thin compact TiO_2 (c-TiO_2) film was spun-coated on FTO substrate with a titanium(IV) diisopropoxide bis(acetylacetonate) solution diluted in butanol (1:10, v/v) and then sintered at 450 °C for 1 h. Over the c-TiO_2 layer, the ZnO layer was spin-cast from ZnO sol–gel solution, at 5000 rpm for 30 s followed by annealing at 300 °C for 1 h. The $MAFAPbI_3$ perovskite layer was deposited according to the aforementioned method. Spiro-OMeTAD as the hole-transporting material (HTM), which solution was prepared by dissolving 29 mg of spiro-OMeTAD, 7 µL of 170 mg mL^{-1} lithium bis(trifluoromethanesulfonyl)imide (Li-TFSI) in acetonitrile, and 11 µL of 4-*tert*-butylpyridine (*t*-BPy), dissolved in 0.4 mL of chlorobenzene and spin-casted at 3000 rpm for 30 s. At last, a thin layer of MoO_3 (10 nm) was thermally evaporated followed by a thick Ag layer (100 nm) over HTM layer under reduced pressure (less than 10^{-6} torr).

Results and discussion

Figure 1a shows the simple all sequential-dip-coating approach for the deposition of mixed cationic ligand-based $MA_xFA_{1-x}PbI_3$ perovskite layers, an aqueous non-halide Pb precursor layer was initially deposited by dipping the ZnO covered c-TiO_2 bilayer electron transport layer (ETL) into the aqueous $Pb(NO_3)_2$ precursor solution.

The $Pb(NO_3)_2$ layer from an aqueous solution rapidly adsorb over ZnO surface and then likely to transform into dark-brown and a blackish-colored film when exposure into pure MAI, FAI or MAI/FAI mixed-precursor solution, confirming the formation of $MAPbI_3$, $FAPbI_3$, or $MA_xFA_{1-x}PbI_3$ perovskite films, respectively, although for a quite short span of time of the 30 s. Nevertheless, since these perovskite layers instantly decomposed by leaving yellowish-colored PbI_2 crystallinity during heating at 120 °C (< 20% relative humidity) [20], we proceeded additional ion-exchange reactions by unreacted $Pb(NO_3)_2$ in these perovskite layers, which is defined as solid-state ion-exchange and reaction (SSIER), so that the more stable $MAPbI_3$, $FAPbI_3$, and $MA_xFA_{1-x}PbI_3$ perovskite films were achieved by applying successive repetition of SSIER cycles (reaction scheme shown in Fig. S9). In this study, the five-type $MA_xFA_{1-x}PbI_3$ ($MA_{0.7}FA_{0.3}PbI_3$, $MA_{0.6}FA_{0.4}PbI_3$, $MA_{0.5}FA_{0.5}PbI_3$, $MA_{0.4}FA_{0.6}PbI_3$, and $MA_{0.3}FA_{0.7}PbI_3$) perovskite layers prepared in different MAI/FAI molar ratios of 0.7/0.3, 0.6/0.4, 0.5/0.5, 0.4/0.6, and 0.3/0.7, respectively, were characterized and compared to $MAPbI_3$ and $FAPbI_3$ perovskite layers prepared MAI and FAI solutions, respectively. Interestingly, these $MA_xFA_{1-x}PbI_3$ perovskite layers were significantly affected by proportions of MAI/

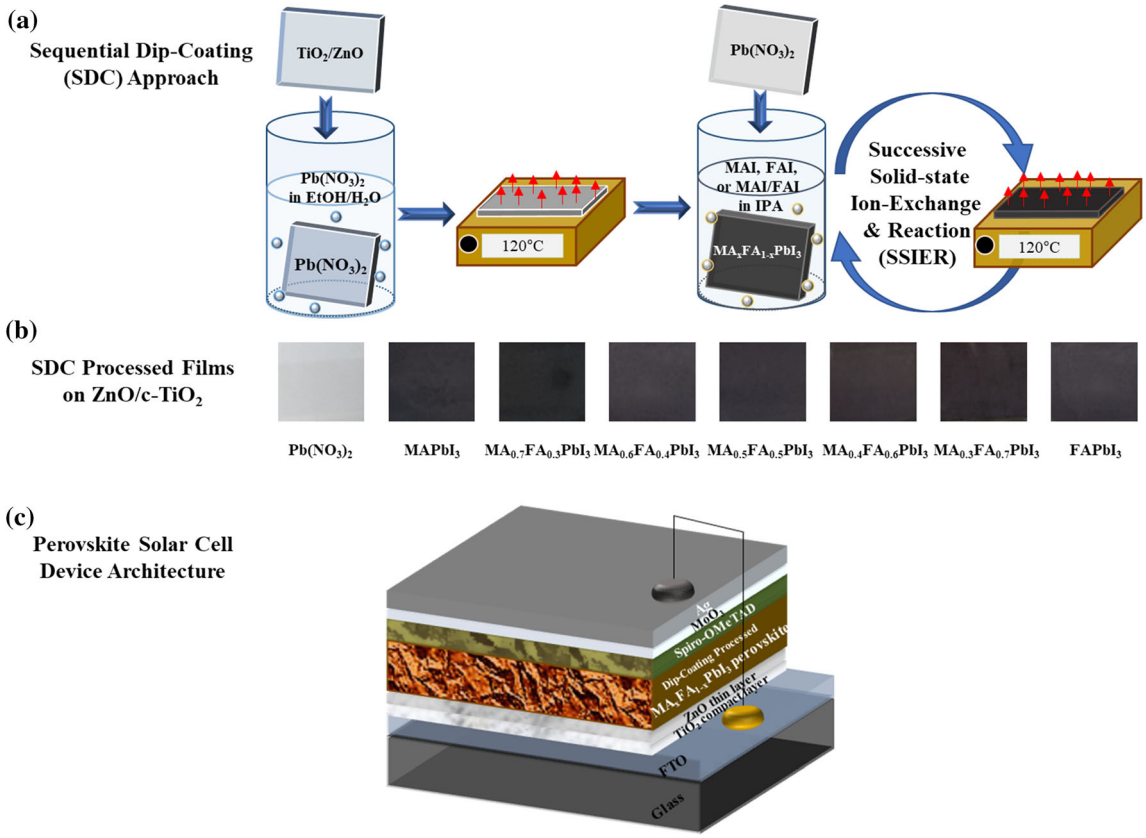

Figure 1 **a** Schematic route of $MA_xFA_{1-x}PbI_3$ perovskite layers prepared by sequential dip-coating approach, **b** their photographic images, and **c** the perovskite solar cell device architecture adapted in this study.

FAI and exhibited stable and much darker blackish-colored films compared to those of $MAPbI_3$ and $FAPbI_3$ as shown in Fig. 1b, and were carried out on perovskite solar cell device for photovoltaic performances as shown in Fig. 1c.

Figure 2 shows the (a) UV–Vis absorption and (b) PL spectra for $MAPbI_3$, $FAPbI_3$ and MAI/FAI mixed-halide $MA_xFA_{1-x}PbI_3$ perovskite films prepared on ZnO/c-TiO_2/FTO substrate. All perovskite films were prepared under controlled air humidity environment of not more than 20% and exhibited the distinctive absorption behavior of $MAPbI_3$ and $FAPbI_3$ perovskites with onset points of ~ 750 nm, ~ 825 nm, respectively [15, 20], as shown in Fig. 2a. The absorption edge wavelength for $FAPbI_3$-based perovskite materials was found to be longer than that of pure $MAPbI_3$-based perovskite materials. The related optical band-gap of $MAPbI_3$- and $FAPbI_3$-based perovskite materials was found to be comparable to the previously published reports of < 1.55 eV and < 1.48 eV, respectively [22]. Meanwhile, it was realized that $FAPbI_3$ films deposited in FAI precursor solution led to the higher light absorption efficiency at a wavelength range of below 550 nm when their baselines were adjusted to a ~ 850 nm, indicating the yellowish δ-$FAPbI_3$ phase [20]. Interestingly, we investigated that the optical characteristics of $MA_xFA_{1-x}PbI_3$ perovskites were meaningfully affected by modulating the MAI/FAI molar ratios. The lower band-gap of $FAPbI_3$-based perovskite materials indicates their lower symmetry than that of $MAPbI_3$-based perovskite, which can be adjusted by varying the FAI concentration into the MAI to form an efficient mixture solution to broaden the spectral response range. The higher FAI concentration in the FAI/MAI mixed halide solution led to turbid and dark blackish perovskite layers, thus producing a non-uniform absorption behavior by light scattering in the UV–Vis absorption spectra. Among them, $MA_{0.5}FA_{0.5}PbI_3$ perovskite film fabricated in MAI/FAI (1/1 molar ratio) solution exhibited a much higher light-absorption efficiency compared to those of other concentration ratios, indicating superior surface crystallinity of perovskite

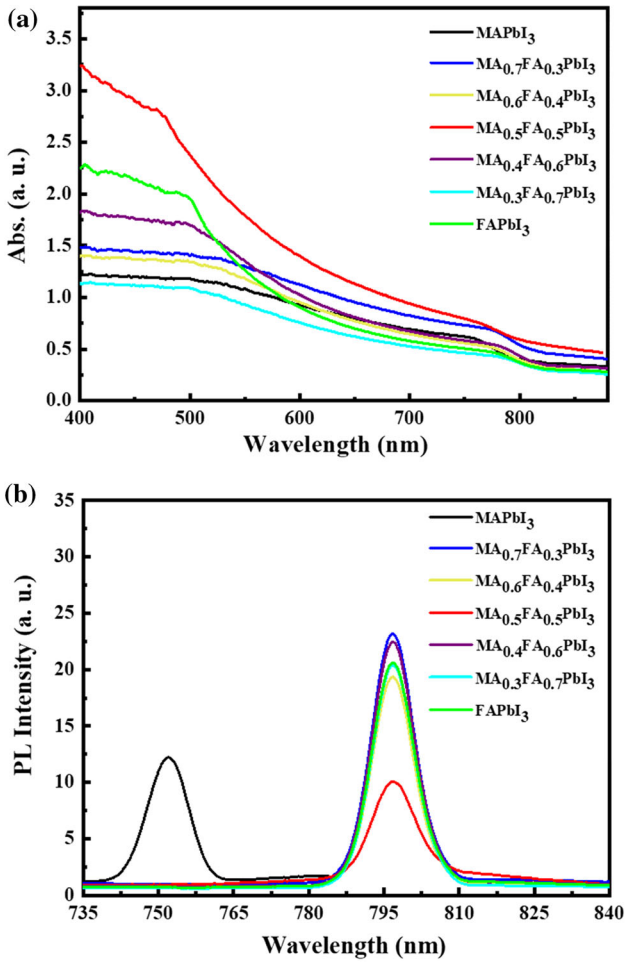

Figure 2 **a** UV–Vis absorption and **b** photoluminescence (PL) spectra for $MAPbI_3$, $FAPbI_3$ and MAI/FAI mixed-halide $MA_xFA_{1-x}PbI_3$ perovskite films prepared on ZnO/c-TiO_2/FTO substrate with MAI (black), FAI (green), and MAI/FAI mixed solutions with various molar ratios (0.7/0.3 (blue), 0.6/0.4 (yellow), 0.5/0.5 (red), 0.4/0.6 (purple), and 0.3/0.7 (cyan)) by all simple dip-coating approach.

films. Meanwhile, the $MAPbI_3$ and $FAPbI_3$ perovskite films exhibited typical PL intense peaks around 751 and 796 nm but the $MA_xFA_{1-x}PbI_3$ perovskite films presented PL intense peaks around 796 nm similar to that of $FAPbI_3$ not $MAPbI_3$ [3, 23]. From these results, we could expect that the characteristics of $MA_xFA_{1-x}PbI_3$ perovskite films fabricated in MAI/FAI mixture solution might be comparable to those of $FAPbI_3$. Interestingly, the $MA_{0.5}FA_{0.5}PbI_3$ perovskite film exhibited the lowest PL intensity value than those of $FAPbI_3$ and $MAPbI_3$ as well as other subjected MAI/FAI solutions as shown in Fig. 2b. This indicates that $MA_{0.5}FA_{0.5}PbI_3$ perovskite film shows better charge transfer behavior into the ZnO/c-TiO_2 ETL layer so that lead to superior device performances in PrSC.

Regarding these results, we realized the surface morphologies of the aforementioned $MAPbI_3$, $FAPbI_3$ and $MA_xFA_{1-x}PbI_3$ perovskite films deposited on ZnO/c-TiO_2/FTO substrate. Figure 3 shows the FESEM surface morphologies of $MAPbI_3$, $FAPbI_3$ and $MA_xFA_{1-x}PbI_3$ perovskite films converted from (a) $Pb(NO_3)_2$ film adsorbed on ZnO/c-TiO_2/FTO substrate with (b) MAI, MAI/FAI mixed solutions with various molar ratios ((c) 0.7/0.3, (d) 0.6/0.4, (e) 0.5/0.5, (f) 0.4/0.6, and (g) 0.3/0.7), and (h) FAI by all simple dip-coating approach.

The $Pb(NO_3)_2$ film was readily prepared by dipping the ZnO/c-TiO_2/FTO substrate into an aqueous halide-free $Pb(NO_3)_2$ precursor solution, ensuring the particulate morphology with superior surface coverages as shown in Fig. 3a. The stable $MAPbI_3$, $FAPbI_3$ and $MA_xFA_{1-x}PbI_3$ perovskite films were prepared via simple all-dip-coating deposition along with the successful SSIER approach with this $Pb(NO_3)_2$ layer. These perovskite films originated mainly from $Pb(NO_3)_2$ particulate and the formed surface crystallinity possess sub-micron-sized crystals with good surface topology on ZnO/c-TiO_2/FTO. These formed morphologies help for an efficient charge transportation and have ability to suppress interfacial recombination between the electron transporting layer (ETL) and hole transporting layer (HTL), contemplating an efficient device performances of PrSCs. Particularly, we realized that their grain size and grain boundaries were mainly affected by the dipping solution condition such as cationic species or molar ratios of MAI/FAI as shown in Fig. 3b–h. Also, the dip-coating processed $FAPbI_3$ exhibited the larger grain size than that of $MAPbI_3$ films, and the lower composition of FAI in MAI/FAI solution leads to the more cubic-like crystal structures of $MA_xFA_{1-x}PbI_3$ perovskite films, providing turbid and non-uniform absorption behavior by light scattering in the UV–Vis absorption spectra as shown in Fig. 2a. Moreover, the rod-like structures which were attributed mainly as photo-inactive hexagonal δ-phase were partially observed in dip-coating processed $FAPbI_3$ films, they were not detected in $MA_xFA_{1-x}PbI_3$ perovskite films. These note that the MAI/FAI mixed composition can significantly affect the cubic α-phase growth preferred thermodynamically in the $FAPbI_3$ perovskite crystallization. Thus, we characterized the crystallinity of perovskite structures via XRD patterns of

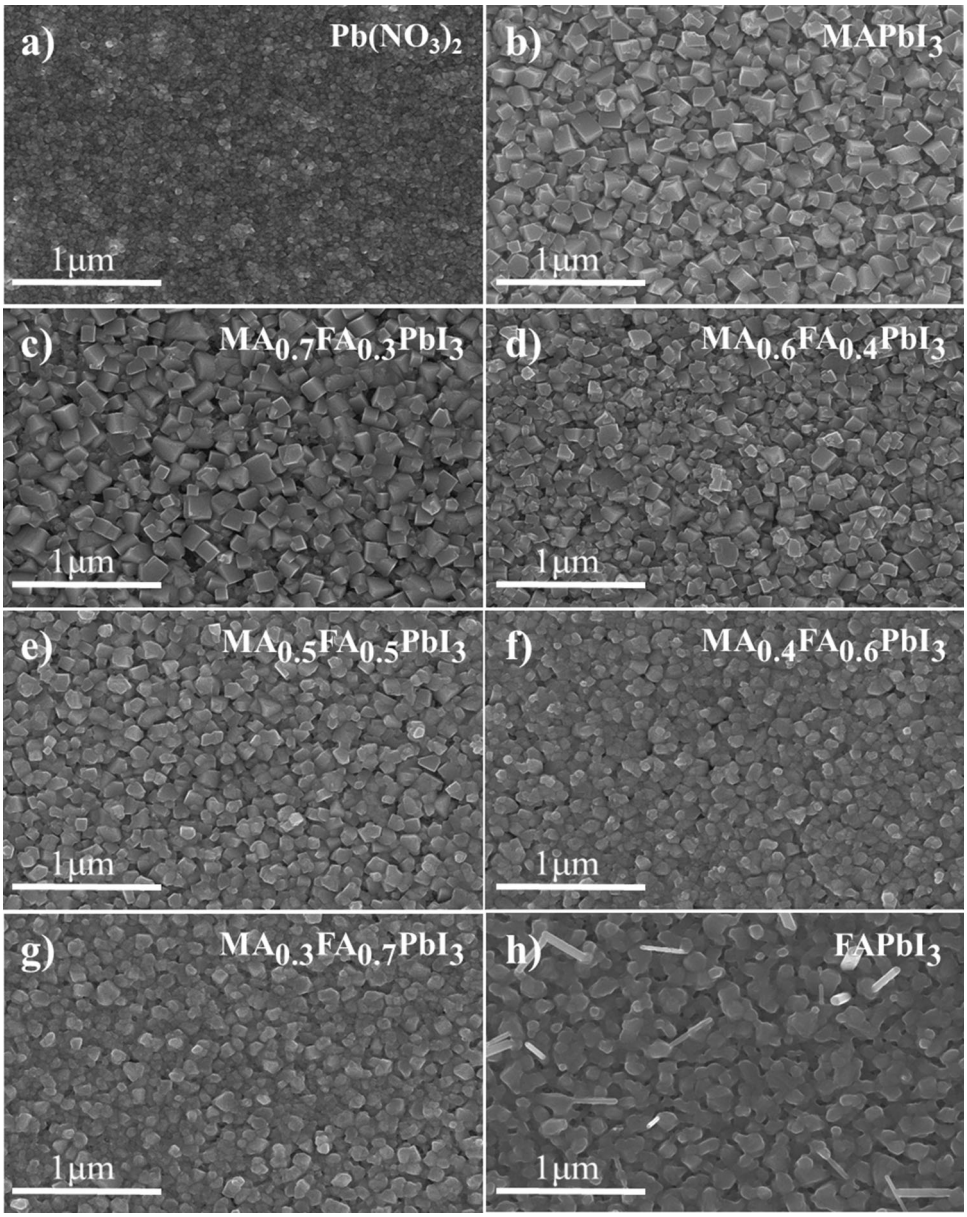

Figure 3 The FESEM surface morphologies of $MAPbI_3$, $FAPbI_3$ and $MA_xFA_{1-x}PbI_3$ perovskite films converted from **a** $Pb(NO_3)_2$ film adsorbed on ZnO/c-TiO_2/FTO substrate with **b** MAI, MAI/FAI mixed solutions with various molar ratios (**c** 0.7/0.3, **d** 0.6/0.4, **e** 0.5/0.5, **f** 0.4/0.6, and **g** 0.3/0.7), and **h** FAI by all simple dip-coating approach.

the aforementioned $MA_xFA_{1-x}PbI_3$ films in which the FA and MA cations are simultaneously intercalated and compared to those of $MAPbI_3$ and $FAPbI_3$ films [21].

Figure 4 shows (a) the XRD patterns of $MAPbI_3$, $FAPbI_3$ and $MA_xFA_{1-x}PbI_3$ films prepared on ZnO/c-TiO_2/FTO substrate with MAI (black), FAI (green), and MAI/FAI mixed solutions with various molar ratios (0.7/0.3 (blue), 0.6/0.4 (yellow), 0.5/0.5 (red), 0.4/0.6 (purple), and 0.3/0.7 (cyan)) by all simple dip-coating approach and (b) the correlated perovskite conversion factors. As shown in Fig. 4a, these films presented usual XRD patterns of $MAPbI_3$ and α-$FAPbI_3$ crystalline structures with intense peaks at $2\theta = 14.2°$ and 13.8°, respectively, relates to (001) diffraction planes [2]. The specific crystallinity peaks for PbI_2 and δ-$FAPbI_3$ (100) were observed at $2\theta = 12.7°$ and 11.8°, correspondingly. Interestingly, although dip-coating processed $FAPbI_3$ films obviously exhibited intense peaks of δ-$FAPbI_3$ (100) at $2\theta = 11.8°$ as well as α-$FAPbI_3$ (100) at $2\theta = 13.8°$, there is no any indication of δ-$FAPbI_3$ crystalline structures in XRD pattern of $MA_xFA_{1-x}PbI_3$ films [21, 22]. These results could be well correlated with those observed in SEM surface morphologies of Fig. 2. Moreover, we observed the diffraction peak

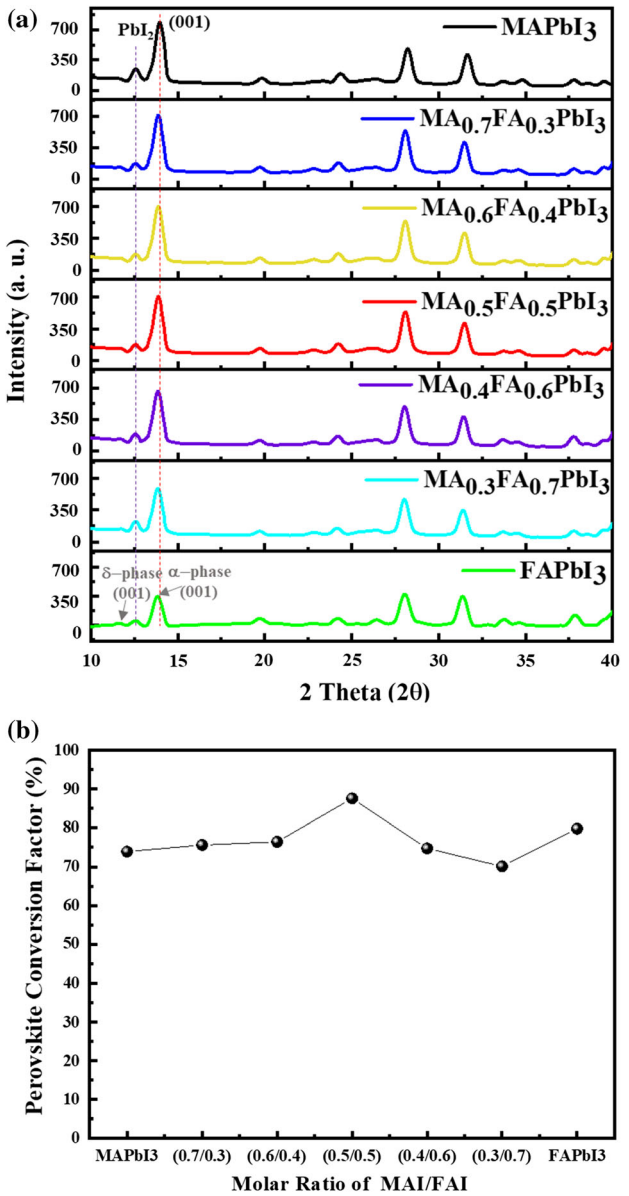

Figure 4 **a** The XRD patterns of $MAPbI_3$, $FAPbI_3$ and $MA_xFA_{1-x}PbI_3$ films prepared on ZnO/c-TiO_2/FTO substrate with MAI (black), FAI (green), and MAI/FAI mixed solutions with various molar ratios (0.7/0.3 (blue), 0.6/0.4 (yellow), 0.5/0.5 (red), 0.4/0.6 (purple), and 0.3/0.7 (cyan)) by all simple dip-coating approach and (**b**) the correlated perovskite conversion factors.

shifting behavior at very small angles by increasing the FAI ratio in the MAI/FAI solutions. This might be caused by the lattice size of perovskite increased steadily by the large-sized FA cation compared to MA cation [22].

Based on these XRD patterns, we qualitatively evaluated the SSIER processed perovskite conversion factors (C_{MAPbI3}, C_{FAPbI3}, and $C_{MAxFA1-xPbI3}$) from PbI_2 intermediates into $MAPbI_3$, $FAPbI_3$, and $MA_xFA_{1-x}PbI_3$ perovskite structures, respectively, by using peak intensities of PbI_2 and perovskites at 2θ = 12.6° and 13.8°–14.02°, respectively [15–20].

$$C_{perov} = I_{PbI2}/(I_{PbI2} + I_{perov}) \quad (1)$$

As shown in Fig. 4b, the perovskite conversion factor, C_{perov} values were significantly affected by the dipping solution condition such as cationic species or molar ratios of MAI/FAI. The $MA_{0.5}FA_{0.5}PbI_3$ perovskite film exhibited the higher conversion value compared to those of $MAPbI_3$, $FAPbI_3$, and other $MA_xFA_{1-x}PbI_3$ perovskites. These results indicate that the competitive insertion between MA and FA cations in perovskite crystal lattice might be closely correlated with the composition ratio in MAI/FAI mixed solution, affecting perovskite crystal growth kinetics [21–23].

Afterward, we investigated the efficient photovoltaic device performances for PrSCs with the aforementioned $MAPbI_3$, $FAPbI_3$, and $MA_xFA_{1-x}PbI_3$ perovskites sequentially deposited from aqueous $Pb(NO_3)_2$. The n-i-p-type PHJ configuration of FTO/c-TiO_2/ZnO/Perovskite/HTM/MoO_3/Ag was fabricated. The relative conductivity as well as efficiency of the used HTM (spiro-OMeTAD) was boosted by doping with different additives like Li-TFSI and *t*-BPy. Figure 5 shows (a) the current–voltage (*J*–*V*) curves under an AM 1.5 irradiation (100 mW cm^{-1}) for the efficiently fabricated $MAPbI_3$, $FAPbI_3$, and $MA_xFA_{1-x}PbI_3$ perovskite layers fabricated with MAI (black), FAI (green), and five MAI/FAI mixed solutions (0.7/0.3 (blue), 0.6/0.4 (yellow), 0.5/0.5 (red), 0.4/0.6 (purple), and 0.3/0.7 (cyan)) and (b) the hysteresis behavior of the *J*–*V* curves for the PrSCs devices fabricated with the $MA_{0.5}FA_{0.5}PbI_3$ perovskites. The SEM cross-sectional image can be found in Fig. S8. The evaluation of photovoltaic performances of the fabricated devices in optimized fabrication condition was proceeded by evaluating more than 200 individual PrSCs devices. The obtained device performance distribution during these processes is shown in Figs. S1–S7 and the efficient device performances in each condition are also summarized in Table S1.

As shown in Fig. 5a, we have realized efficient device performances for PrSCs for the very first time with dip-all-coated processed $MA_{0.5}FA_{0.5}PbI_3$

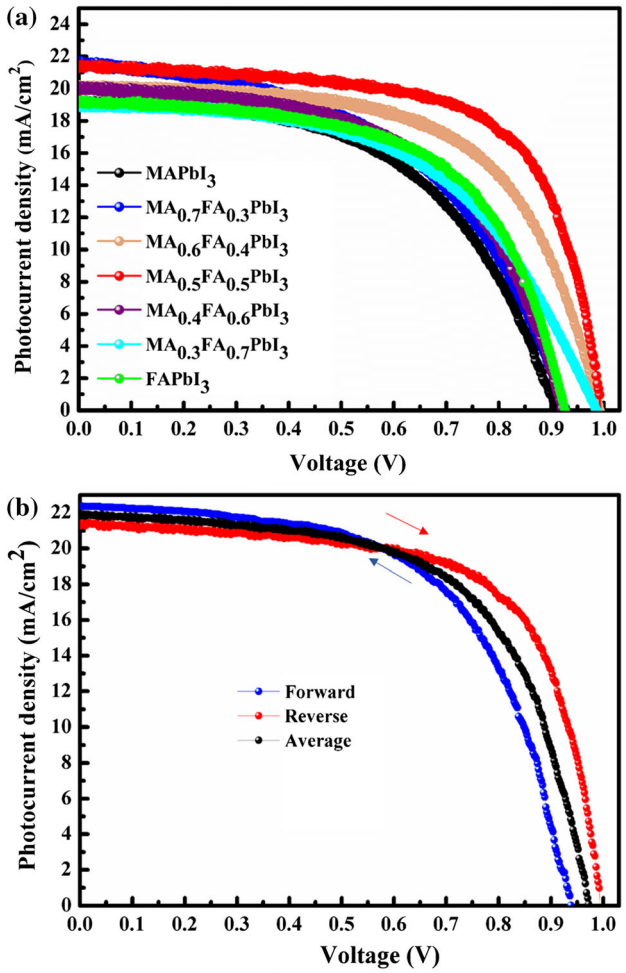

Figure 5 **a** The current–voltage (*J–V*) curves under an AM 1.5 irradiation (100 mW cm^{-1}) for most efficient PrSCs based on $MAPbI_3$, $FAPbI_3$, and $MA_xFA_{1-x}PbI_3$ perovskite layers fabricated with MAI (black dotted line), FAI (green dotted line), and five MAI/FAI mixed solutions (0.7/0.3 (blue dotted line), 0.6/0.4 (yellow dotted line), 0.5/0.5 (red dotted line), 0.4/0.6 (purple dotted line), and 0.3/0.7 (cyan dotted line)) and (**b**) the hysteresis behavior of the *J–V* curves in both scan directions for the PrSCs devices fabricated with the $MA_{0.5}FA_{0.5}PbI_3$ perovskite layer.

perovskites and the PCE values are pretty notable with a maximum/average of 14.1%/13.69% with a J_{sc} of 21.2 mA cm^{-2}, open-circuit voltage (V_{oc}) of 0.99 V, and fill factor (*F.F*) of 0.67. These values exhibited much better performance in-contrast to $MAPbI_3$ and $FAPbI_3$ devices carried out under the same conditions; the PCEs of 9.30%/9.07% (with J_{sc} = 19.24 mA cm^{-2}, V_{oc} = 0.87 V, and *F.F* = 0.56) and 10.81%/10.72% (with J_{sc} = 19.09 mA cm^{-2}, V_{oc} = 0.93 V, and *F.F* = 0.61), respectively. These outcomes might be because of the high perovskite conversion factors, superior surface morphology, and better crystallinity due to photo-inactive constituents such as PbI_2 and δ-$FAPbI_3$ in perovskite layers which may hinder efficient charge transportations [24]. The PrSCs devices with $MA_{0.7}FA_{0.3}PbI_3$, $MA_{0.6}FA_{0.4}PbI_3$, $MA_{0.4}FA_{0.6}PbI_3$, and $MA_{0.3}FA_{0.7}PbI_3$ perovskite layers also showed the efficient PCEs of 10.1%/9.61% (with J_{sc} = 21.5 mA cm^{-2}, V_{oc} = 0.93 V, and *F.F* = 0.50), 12.42%/12.20% (with J_{sc} = 19.16 mA cm^{-2}, V_{oc} = 1.01 V, and *F.F* = 0.64), 10.37%/10.09% (with J_{sc} = 19.98 mA cm^{-2}, V_{oc} = 0.92 V, and *F.F* = 0.56), and 10.1%/9.72% (with J_{sc} = 19.1 mA cm^{-2}, V_{oc} = 0.99 V, and *F.F* = 0.53), respectively. While the *J-V* hysteretic behavior mainly depends on the scan directions and often showed in a typical n-i-p-type PrSC devices mainly while using TiO_2 electrode due to various charge extraction as well as charge transportation rates of electrons and holes parted from the excitons [25]. As shown in Fig. 5b, the PrSCs presented minor differences with deviation in J_{sc} values, whereas V_{oc} and *F.F* values reduced slightly in the forward direction. However, the average PCE calculated in both directions is approximately 5% lowered than that obtained in the reverse direction. These performance values are also summarized in Table S1. These results might be caused by interfacial recombination with the TiO_2 electrode and due to the impurity issues of PbI_2, grain boundary, and a little pin-holes observed in surface coverage of perovskite film [15–20, 26, 27].

Figure 6 shows (a) EQE and (b) the operational stability for the best-performing PrSC device with $MA_{0.5}FA_{0.5}PbI_3$ perovskite layer prepared by a sequential dip-coating approach. The stability of the champion devices was calculated without any encapsulation under N_2 atmosphere. As shown in Fig. 6, the PrSC devices with $MA_{0.5}FA_{0.5}PbI_3$ perovskite layer presented good EQEs in their light-absorption area, where integrated photo-current correlates well with the J_{sc} values and also exhibited an outstanding operational stability without any noticeable lowering of photo-voltaic performances for 400 h.

Conclusion

In summary, we have efficiently presented a simple preparation of highly efficient mixed cationic lead halide, $MA_xFA_{1-x}PbI_3$ perovskite films by employing all-sequential dip-coating deposition from aqueous

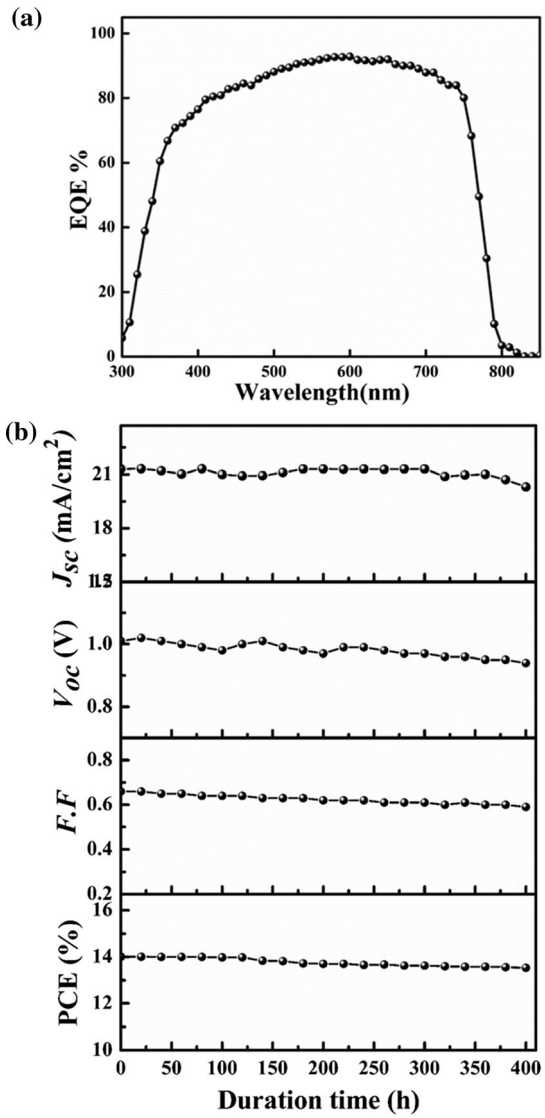

Figure 6 **a** EQE and **b** the operational stability for the best-performing PrSC device (under N_2 atmosphere) with $MA_{0.5}FA_{0.5}PbI_3$ perovskite layer prepared by a sequential dip-coating approach.

lead precursor to develop the facile and environmentally friendly approaches for high-efficiency PrSCs. In this study, we modulated the dipping solution condition such as cationic species such as MAI and FAI or molar ratios of MAI/FAI mixture. The $MA_xFA_{1-x}PbI_3$ perovskite films prepared from MA and FA mixed cationic ligand coordination exhibited better characteristics compared to those of $MAPbI_3$ and $FAPbI_3$ with MA and FA ligand, respectively, carried out under the same conditions. The high crystal conversion and growth factors from precursor, surface morphology and crystallinity were demonstrated in the $MA_xFA_{1-x}PbI_3$ perovskite films. Also, since the most efficient characteristics of perovskite films were mainly observed in $MA_{0.5}FA_{0.5}PbI_3$ perovskite films, we speculated that the competitive insertion between MA and FA cations in perovskite crystal lattice might be closely correlated with the composition ratio in MAI/FAI mixed solution. Moreover, the outstanding device performances with improved stability with a PCE of ~ 14.1% in PrSC devices with the all-dip-coating processed $MA_{0.5}FA_{0.5}PbI_3$ perovskite layer. These results let us believe that this all-dip-coating process might add a good significance to the development and the fascinating deposition technology of perovskite film to dominate the spin-coating strategy which has a size restriction and the use of very toxic and detrimental organic solvents for highly performing PrSCs.

Supporting information

The additional experimental part (materials and instrument) and the performance distributions of PrSCs fabricated based on all-dip-coating processed on $MAPbI_3$, $FAPbI_3$, and $MA_xFA_{1-x}PbI_3$ perovskite layers and the values of best device performance are available in supporting information.

Acknowledgements

This work was financially supported by Chosun University, 2021

Declarations

Conflict of interest The authors declared that they have no conflicts of Interests.

Supplementary Information: The online version contains supplementary material available at https://doi.org/10.1007/s10853-022-06867-9.

References

[1] Okamoto Y, Yasuda T, Sumiya M, Suzuki Y (2018) Perovskite solar cells prepared by advanced three-step method using additional HC (NH2) 2I spin-coating: efficiency improvement with multiple bandgap structure. ACS Appl

Energy Mater 3:1389–1394. https://doi.org/10.1021/acsaem.8b00178

[2] Yang Z, Chueh C, Liang PW, Crump M, Lin F, Zhu Z, Jen K-YA (2016) Effects of formamidinium and bromide ion substitution in methylammonium lead triiodide toward high-performance perovskite solar cells. Nano Energy 22:328–337. https://doi.org/10.1016/j.nanoen.2016.02.033

[3] Chen J, Xu J, Xiao L, Zhang B, Dai S, Yao J (2017) Mixed-organic-cation $(FA)_x(MA)_{1-x}PbI3$ planar perovskite solar cells with 16.48% efficiency via a low-pressure vapor-assisted solution process. ACS Appl Mater Interfaces 3:2449–2458. https://doi.org/10.1021/acsami.6b13410

[4] Zhao YL, Wang JF, Zhao BG, Jia CC, Mou JP, Zhu L, Song J, Quan X, Qiang YH (2018) Fabrication of mixed perovskite organic cation thin films via controllable cation exchange. Chin Phys B 27(2):024208. https://doi.org/10.1088/1674-1056/27/2/024208

[5] Aharon S, Dymshits A, Rotem A, Etgar L (2015) Temperature dependence of hole conductor free formamidinium lead iodide perovskite based solar cells. J Mater Chem A 17:9171–9178. https://doi.org/10.1039/C4TA05149A

[6] Xiao M, Zhao L, Shoubin W, Yanyan L, Binghai D, Shimin W (2018) Application of mixed-organic-cation for high performance hole-conductor-free perovskite solar cells. J Colloid Interface Sci 510:118–126. https://doi.org/10.1016/j.jcis.2017.09.056

[7] Salado M, Calio L, Berger R, Kazim S, Shahzada A (2016) Influence of the mixed organic cation ratio in lead iodide based perovskite on the performance of solar cells. Phys Chem Chem Phys 39:27148–27157. https://doi.org/10.1039/C6CP03851D

[8] Piatkowski P, Cohen B, Ponseca CS Jr, Salado M, Samrana K, Shahzada A, Sundström V (2016) Unraveling charge carriers generation, diffusion, and recombination in formamidinium lead triiodide perovskite polycrystalline thin film. J Phys Chem Lett 7:204–210. https://doi.org/10.1021/acs.jpclett.5b02648

[9] Han Q, Sang-Hoon B, Pengyu S, Hsieh YT, Yang Y, Rim YS, Hongxiang Z et al (2016) Single crystal formamidinium lead iodide (FAPbI3): insight into the structural, optical, and electrical properties. Adv Mater 28(11):2253–2258. https://doi.org/10.1002/adma.201505002

[10] Zhang Y, Grancini G, Feng Y, Asiri AM, Nazeeruddin MK (2017) Optimization of stable quasi-cubic $FA_xMA_{1-x}PbI3$ perovskite structure for solar cells with efficiency beyond 20%. ACS Energy Lett 2(4):802–806. https://doi.org/10.1021/acsenergylett.7b00112

[11] Adnan M, Kim HS, Jeong H, Ko HM, Woo SK, Lee JK (2017) Efficient synthesis and characterization of solvatochromic fluorophore. Bull Korean Chem Soc 38(9):1052–1057. https://doi.org/10.1002/bkcs.11219

[12] Aguiar JA, Wozny S, Holesinger TG, Aoki T, Patel MK, Yang M, Berry JJ (2016) In situ investigation of the formation and metastability of formamidinium lead tri-iodide perovskite solar cells. Energy Environ Sci 9(7):2372–2382. https://doi.org/10.1039/C6EE01079B

[13] Eperon EG, Beck CE, Snaith HJ (2016) Cation exchange for thin film lead iodide perovskite interconversion. Mater Horiz 3(1):63–71. https://doi.org/10.1039/C5MH00170F

[14] Smecca E, Numata Y, Deretzis I, Pellegrino G, Boninelli S, Miyasaka T, La Magna A, Alessandra A (2016) Stability of solution-processed MAPbI 3 and FAPbI 3 layers. Phys Chem Chem Phys 18(19):13413–13422. https://doi.org/10.1039/C6CP00721J

[15] Adnan M, Lee JK (2018) All sequential dip-coating processed perovskite layers from an aqueous lead precursor for high efficiency perovskite solar cells. Sci Rep 8(1):1–10. https://doi.org/10.1038/s41598-018-20296-2

[16] Adnan M, Lee JK (2020) Highly efficient planar heterojunction perovskite solar cells with sequentially dip-coated deposited perovskite layers from a non-halide aqueous lead precursor. RSC Adv 10(9):5454–5461. https://doi.org/10.1039/C9RA09607H

[17] Adnan M, Irshad Z, Lee JK (2020) Facile all-dip-coating deposition of highly efficient (CH 3) 3 $NPbI_{3-x}Cl_x$ perovskite materials from aqueous non-halide lead precursor. RSC Adv 10(48):29010–29017. https://doi.org/10.1039/D0RA06074G

[18] Adnand M, Kim HS, Jeong H, Ko HM, Woo SK, Lee JK (2017) Efficient synthesis and characterization of solvatochromic fluorophore. Bull Korean Chem Soc 38(9):1052–1057. https://doi.org/10.1002/bkcs.11219

[19] Irshad Z, Adnan M, Lee JK (2020) Efficient planar heterojunction inverted perovskite solar cells with perovskite materials deposited using an aqueous non-halide lead precursor. Bull Korean Chem Soc 41(9):937–942. https://doi.org/10.1002/bkcs.12092

[20] Irshad Z, Adnan M, Lee JK (2022) Controlling phase and morphology of all-dip-coating processed HC(NH2)2PbI3 perovskite layers from an aqueous halide-free lead precursor. J Phys Chem Solids 160:110374. https://doi.org/10.1016/j.jpcs.2021.110374

[21] Gerardo GG, Virgüez-Amaya O, Otálora-Bastidas C, Calderón-Triana C, Quiñones-Segura C (2020) Synthesis and optimization of properties of thin films of $FA_x(MA_{1-X})PbI3$ grown by spin coating with perovskite structure to be used as active layer in hybrid solar cells. Revista UIS Ingenierías 19(1):87–94. https://doi.org/10.18273/revuin.v19n1-2020008

[22] Slimi B, Mollar M, Ben Assaker I, Kriaa I, Chtourou R, Marı B (2016) Perovskite FA1-xMAxPbI3 for solar cells: films formation and properties. Energy Procedia 102:87–95. https://doi.org/10.1016/j.egypro.2016.11.322

[23] Zhang Y, Grancini G, Feng Y, Asiri AM, Nazeeruddin MK (2017) Optimization of stable quasi-cubic $FA_xMA_{1-x}PbI3$ perovskite structure for solar cells with efficiency beyond 20%. ACS Energy Lett 2(4):802–806. https://doi.org/10.1021/acsenergylett.7b00112

[24] Huang Y, Li L, Liu Z, Jiao H, He Y, Wang X, Zhu R et al (2017) The intrinsic properties of $FA_{(1-x)}MA_xPbI$ 3 perovskite single crystals. J Mater Chem A 5(18):8537–8544. https://doi.org/10.1039/C7TA01441D

[25] Unger LE, Hoke TE, Bailie DC, Nguyen HY, Bowring RA, Heumuller T, Christoforo GM, McGehee DM (2014) Hysteresis and transient behavior in current-voltage measurements of hybrid-perovskite absorber solar cells. Energy Environ Sci 7(11):3690. https://doi.org/10.1039/C4EE02465F

[26] Liu L, Zuo C, l, (2021) Ding, Self-spreading produces highly efficient perovskite solar cells. Nano Energy 90:106509. https://doi.org/10.1016/j.nanoen.2021.106509

[27] Ke L, Ding L (2021) Perovskite crystallization. J Semicond 42(8):080203. https://doi.org/10.1088/1674-4926/42/8/080203